Energetics of Self-Interstitial Clusters in Si

N. E. B. Cowern, G. Mannino,* P. A. Stolk, F. Roozeboom, H. G. A. Huizing, and J. G. M. van Berkum

Philips Research Laboratories, Professor Holstlaan 4, 5656 AA Eindhoven, The Netherlands

F. Cristiano and A. Claverie

CEMES/CNRS, BP 4347, 31055 Toulouse Cedex, France

M. Jaraíz

Departamento Electricidad y Electronica, ETSIT Campus Miguel Delibes, 47011 Valladolid, Spain

The transient supersaturation in a system undergoing Ostwald ripening is related to the cluster formation energy E_{fc} as a function of cluster size n. We use this relation to study the energetics of self-interstitial clusters in Si. Measurements of transient enhanced diffusion of B in Si-implanted Si are used to determine $S(t)$, and inverse modeling is used to derive $E_{fc}(n)$. For clusters with $n > 15$, $E_{fc} \approx 0.8$ eV, close to the fault energy of {113} defects. For clusters with $n < 10$, E_{fc} is typically 0.5 eV higher, but stabler clusters exist at $n \approx 4$ ($E_{fc} \approx 1.0$ eV) and $n \approx 8$ ($E_{fc} \approx 0.6$ eV). [S0031-9007(99)09311-4]

Diffusion of dopant impurities in semiconductors is strongly influenced by the thermal behavior of self-interstitial clusters, nucleated as a result of nonequilibrium processing steps such as ion implantation. These clusters, which have a high formation energy, anneal rapidly and produce transient enhanced diffusion (TED), most notably of dopants such as B, P, and In in Si, and host atoms in compound semiconductor superlattices.

Recently, considerable efforts have been devoted to understanding the annealing kinetics of rodlike "{113}" interstitial clusters [1,2], which play an important role in TED [2–6]. However, almost nothing is known about the smaller precursor clusters that nucleate and grow into {113} defects, and which may also play a role in TED [3]. Theoretical study of such clusters is a major challenge, and only the very smallest clusters, the di-interstitial [7] and the 4-cluster [8], and some aspects of larger {113} defects [1,9] have been considered. Experimentally even less is known, although the growth and decay of cluster-related deep-level states, consistent with Ostwald ripening (OR) of small interstitial clusters, has recently been reported [10].

In this Letter we use a novel experimental approach to determine the formation energies, E_{fc}, of these precursor clusters. The approach relies on two consecutive steps: accurate TED measurements using B-doped marker layers, to determine the transient interstitial supersaturation $S(t)$ during cluster ripening, and inverse modeling of the ripening process, to extract from $S(t)$ the fundamental physical information on E_{fc}. For the largest clusters the model prediction for the mean cluster size, $\bar{n}$, is tested experimentally using transmission electron microscopy (TEM).

We first discuss the experimental aspects. A 2.5 μm intrinsic Si layer containing thin, lightly B-doped marker layers at depths of 0.9 and 1.3 μm is epitaxially grown on a lightly n-type doped substrate using an ASM Epsilon One CVD reactor. After growth, the wafer is implanted with 40 keV $2 \times 10^{13}/\text{cm}^2$ ^{28}Si ions, cut into small samples, cleaned, and annealed in dry N$_2$ at 600, 700, and 800 °C for times in the range 1 s to 20 h. Rapid thermal annealing (RTA) is used for anneal times up to 5 h, and furnace annealing is used for the time range 10–20 h. The absolute RTA temperature, calibrated by thermocouple, is confirmed to within 4 °C by measuring the regrowth rate of Ge-amorphized Si. Temperature overshoot at the start of RTA is less than 1.5 °C.

After annealing, the B concentration profiles in the samples are analyzed by secondary-ion mass spectrometry. Typical results are shown in Fig. 1. Significant diffusive broadening occurs within the first seconds of annealing at 600 °C. The profile after 5 s shows exponential tails with a characteristic decay length $\lambda \sim 10$ nm. Such tails play a role in all the measured profiles, though less evident at longer anneal times. This exponential property is known to arise from the interstitial kick-out mechanism of B diffusion [11,12]. About half of the B atoms move during the 5 s anneal, indicating an average kick-out frequency of $\sim 0.1/s$—7 orders of magnitude faster than the equilibrium kick-out rate at 600 °C [11]. The exponential tails signify that the B atoms are kicked out, migrate, and return to a substitutional site, in a much shorter time span than the interval between kick-out events [12]. Under these conditions the B diffusivity enhancement is directly proportional to $S(t)$.

The evolution $S(t)$ is extracted as follows. The as-grown profile is convolved with the B diffusion function $f(x, t)$ described in Ref. [12], and fitted to the measured diffused profile to extract the diffusive broadening $w = \sqrt{2 \int D \, dt}$. The average diffusivity D_B over the period

t_{i-1} to t_i is obtained from the relation $2D_B(t_i - t_{i-1}) = w_i^2 - w_{i-1}^2$, and finally $S(t)$ is estimated from $S = D_B/D_B^{eq}$, where D_B^{eq} is the equilibrium diffusivity of B taken from Fair [13].

The extracted values of S are shown in Fig. 2. The data show two phases of enhanced diffusion. An initial phase of ultrafast TED is followed by a sharp drop in S and a lower "plateau" with near-constant S up to time τ, when the transient diffusion rather abruptly ends. The ultrafast phase persists for a much longer time than it takes for free interstitials, I, to diffuse through the measurement structure (<1 s at 600 °C). As we shall see, the ultrafast phase reflects ripening of very small interstitial clusters—precursors in the nucleation of {113} defects.

The plateau region closely matches previous observations of TED driven by {113} defects [2,5,6]. The time scale τ, which represents the survival time of the {113} defect band against loss of I to the surface, is determined by the areal density of I present in the {113} defects, and by the capacity of the crystal to transport them from the defect band to the surface. Assuming the surface is a perfect sink, as evidenced by previous studies [14], the flux to the surface is given by $D_I C_I^* S/L$ where D_I and C_I^* are the diffusivity and equilibrium concentration of I in Si and L ($\approx r_p$, the ion projected range) is the depth of the defect band.

To estimate E_{fc} as a function of n we carry out inverse modeling of the $S(t)$ data using an OR model for interstitial clusters. The model accounts for the capture and emission of I to and from cluster sizes up to a specified cutoff maximum ($n = 250$ in this study) and

includes a loss term due to the flux to the surface. It is assumed that, once the clusters have nucleated, the number of free I in the wafer is always much smaller than the number of clustered I, and $S(t)$ quickly reaches a quasi steady state with respect to the cluster-size distribution. In this case the actual number of free I can be eliminated from the analysis and S can be calculated directly. Simulations with the Monte Carlo atomistic simulator DADOS (diffusion of atomistic defects, object-oriented simulator) [15] confirm the validity of this picture, and show that $S(t)$ is not significantly modified when vacancy clusters are considered. Using the OR model the evolution of the cluster-size distribution N_n and the supersaturation S can be expressed as

$$\frac{dN_n}{dt} = F_{n-1}N_{n-1} - F_nN_n - R_nN_n + R_{n+1}N_{n+1},$$

$$S = \frac{\sum_{n=2}^{\infty} \beta_n R_n N_n}{D_I C_I^* (\sum_{n=2}^{\infty} 4\pi a_n N_n + 1/r_p)},$$

where

$$F_n = 4\pi a_n D_I C_I^* S,$$
$$R_n = (6D_{0n}a_n/\lambda^3)\exp -[E_{diss}(n)]/kT$$

are forward and reverse reaction rates describing the capture and emission of I from clusters of size n. The quantity $E_{diss}(n)$ is the cluster dissociation energy, $E_{diss} = Q - E_{fc}$ where Q is the activation energy of the product $D_I C_I^*$. Furthermore, D_{0n} is the emission prefactor and a_n is the capture radius for I at clusters of size n. The quantity β is the number of free I released by the emission reaction; $\beta = 2$ when $n = 2$, otherwise $\beta = 1$. The term involving r_p accounts for the loss of
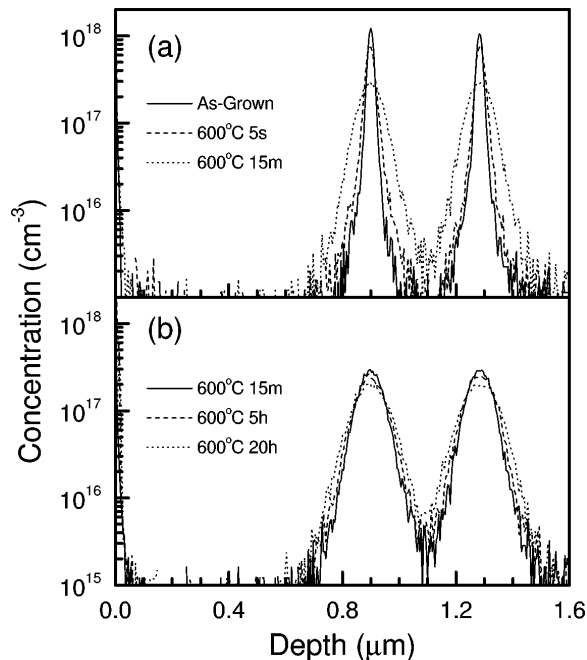

FIG. 1. B concentration profiles before and after annealing for a range of times at 600 °C.
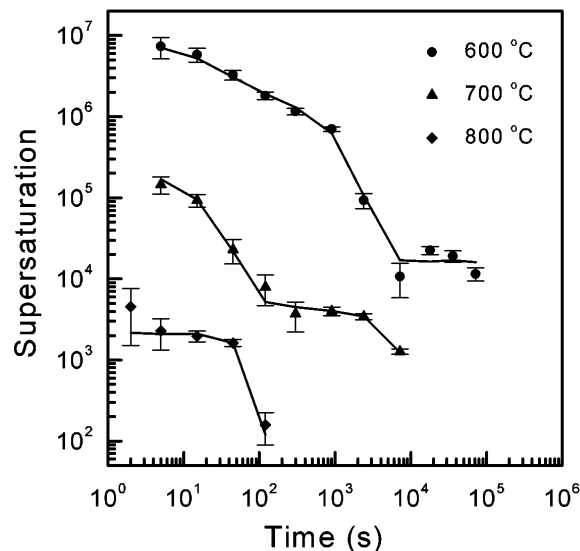

FIG. 2. Interstitial supersaturation, S, as a function of annealing temperature and time. Symbols with error bars represent experimental values with 2σ uncertainties. Curves represent fits using an Ostwald ripening model (see text).

I to the Si surface. Assuming for present purposes that the clusters are elongated planar defects [9], we model each dimer as an independent, uncorrelated, capture site of capture radius λ. This yields a cluster capture radius of $a_n \approx n\lambda/2$. More compact cluster geometries, which cannot be ruled out in the case of small clusters, would cause a sublinear dependence of a_n on n in that size range. We have checked the sensitivity to this assumption by simulating the ripening process with size dependences of $a_n \propto \sqrt{n}$ and $a_n \propto n$ in the size range $n < 10$. This gives rise to a modest variation, less than a factor of 2, in the growth rate of the cluster-size distribution and a small change in the formation energies needed to fit our data.

The OR solver is now embedded in a function minimization routine to extract least-squares-fitted values for the product $D_I C_I^*$ and the variation of E_{fc} as a function of n. $E_{fc}(n)$ is treated as a piecewise-linear function of n, using a sufficient number of nodes to extract the significant information from the data ($\chi^2 \sim 1$). The initial conditions for the simulation are $n = 2$ and $N_2 = \Phi/2$ where Φ is the implant dose. The initial cluster size is based on atomistic simulations. The initial cluster density is chosen on the assumption that I-V recombination has already occurred and only the "+1" interstitials added by the implant contribute significantly to TED. It is unlikely that all vacancies disappear before 1 s at 600 °C; however, atomistic simulations show that the presence of excess vacancies does not significantly influence $S(t)$ during cluster ripening.

To test the consistency of the extracted parameters we fit the data for each temperature separately. The resulting fits are shown in Fig. 2. Excellent agreement is obtained for all three temperatures, including the steep drop in S in the 600 °C curve at $\sim 10^3$ s and the less steep decrease in the 700 °C curve. The extracted parameter $D_I C_I^*$ is of interest as it has not previously been estimated in this low temperature range. Our fitted values are within 40% of an extrapolation from recent isotope self-diffusion data at higher temperatures [16]. This quite close agreement suggests that interstitial motion is an important contribution to self-diffusion, even at these low temperatures. We extract a value of $Q = 4.52 \pm 0.05$ eV.

Our extracted values of E_{fc} are plotted in Fig. 3(a). The value for small clusters ($n < 10$) is typically about 0.5 eV higher than that for larger clusters, but shows strong minima at values of $n \approx 4$ and 8. Strong maxima occur adjacent to the minimum at $n \approx 8$. A near-constant E_{fc} is to be expected for rodlike defects, which have a constant edge energy per unit length, and the value of $E_{fc} = 0.8$ eV ($E_{diss} = 3.7$ eV) agrees with previous measurements of the stability of {113} defects [6]. The behavior at small n is remarkable and requires critical consideration. It is tempting to dismiss it as an artifact of inverse modeling, but we can show that it passes two critical existence tests. First, the same structure emerges

from data at different temperatures, even though the shapes of the $S(t)$ curves are substantially different. This clearly suggests that the extracted structure represents real physics. Second, we completely fail to fit the data when we apply the constraint that E_{fc} must vary monotonically with n. This results in curves that vary smoothly in time, in contrast to the sharp drop seen after 10^3 s at 600 °C. Some kind of rate-limiting step seems to be needed to fit the data.

To show how this occurs we examine the cluster-size evolution obtained using our fitted parameters. The time evolution of the clustered I at 600 °C, obtained from the OR model, is shown in Fig. 3(b). During the first 100 s the average cluster size is well below 10, corresponding to clusters with high E_{fc}. During this period the large step-up in E_{fc} between $n \approx 8$ and 9 leads to recycling of free I via reaction sequences like $I_8 + I \rightarrow I_9$, $I_9 \rightarrow I_8 + I$. The probability of passing the energy maximum at $n \approx 9$
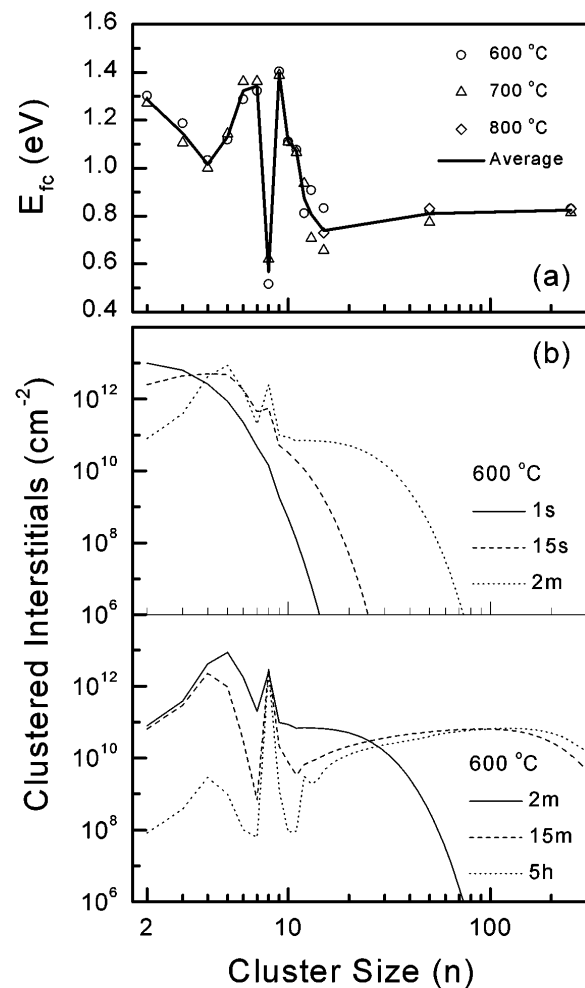

FIG. 3. (a) Formation energies of interstitial clusters, estimated from the OR analysis. Symbols show the values extracted from the $S(t)$ data at each temperature, and the line represents the average result. (b) Time evolution of the cluster-size distribution at 600 °C.

and proceeding to higher cluster sizes decreases rapidly with $S(t)$, as the capture rate for this cluster falls far below its emission rate. This "statistical barrier" provides a rate-limiting step, forcing the buildup of a narrow cluster-size distribution at around $n \approx 8$ during the period 10^2–10^3 s. During the period 10^3–10^4 s the size distribution goes through a major transition as a fraction of "lucky" clusters undergo double capture events and reach sizes ≥ 10. The population of small clusters collapses and further ripening of size-8 clusters is extremely slow. Nearly half of the clustered interstitials remain in clusters of size 8. Larger clusters continue to ripen, producing a broad distribution in the range $n = 10$–200.

A similar evolution, not shown in the figure, occurs at 700 °C. The barrier effect is slightly reduced because the higher flux of I at 700 °C enables more clusters to pass the energy maximum at short times. This leads to a smoother transition to {113} defects than at 600 °C, and a larger number of clusters reach the size range $n > 10$. The predicted average cluster size after 40 m at 700 °C is $\bar{n} = 91$. Corresponding TEM measurements show {113} defects with an average projected length of (4 ± 2) nm, equivalent to $\bar{n} \approx 80 \pm 40$. Measurements at longer times show a rapid decrease in cluster density, matching the drop in S at $t \sim 10^4$ s shown in Fig. 2. At 800 °C the cluster-size evolution is very fast and there is no significant barrier to the formation of {113} defects.

The occurrence of oscillations in $E(n)$ is not necessarily confined to the range $n < 10$. In the {113}-controlled regime, $S(t)$ is largely determined by the defects with the highest E_{fc}, and our analysis does not rule out the existence of a subset of stabler {113} defects. In fact, our analysis for $n < 10$ only encourages speculation that such defects may exist. An obvious candidate would be a {113} defect with a complete row of atoms at each end. However, our analysis does show that E_{fc}, averaged over a sufficient number of adjacent values of n, is almost constant over a wide range of $n > 15$.

We have seen how measurements of $S(t)$ during Ostwald ripening can provide tight constraints on the structure of the formation-energy curve $E_{\text{fc}}(n)$. This may turn out to be a useful research tool in a variety of fields. In our present study of self-interstitial clusters in Si, we observe dramatic fluctuations in $E_{\text{fc}}(n)$ for the first few values of n. Oscillations in E_{fc} are well known in the fields of molecular, atomic, and nuclear physics, but have never before been detected in experiments on defect clusters in solids. Our results show minima in E_{fc} at $n \approx 4$ and 8, reminiscent of Arai's proposal that the basic building block of rodlike defects is a stable size-4 interstitial cluster [8]. Key features of our results are an apparently superstable cluster of size $n_s \approx 8$, with

much less stable adjacent clusters at $n = n_s - 1$ and $n = n_s + 1$, and a transition at $n > 10$ to a broad range of defects with the characteristic energy and microstructure of {113} defects. In conclusion, an analysis of $S(t)$ during Ostwald ripening has provided novel insights into clustering phenomena at the borders between the atomic scale and the length scale accessible to TEM imaging.

*Permanent address: INFM and Dipartimento di Fisica, Università di Catania, Corso Italia 57, 95129 Catania, Italy.

[1] M. Kohyama and S. Takeda, Phys. Rev. B **46**, 12 305 (1992); **51**, 13 111 (1995).

[2] D. J. Eaglesham, P. A. Stolk, H.-J. Gossmann, and J. M. Poate, Appl. Phys. Lett. **65**, 2305 (1994).

[3] N. E. B. Cowern, G. F. A. van de Walle, P. C. Zalm, and D. W. E. Vandenhoudt, Appl. Phys. Lett. **65**, 2981 (1994).

[4] H. G. A. Huizing, C. C. G. Visser, N. E. B. Cowern, P. A. Stolk, and R. C. M. de Kruif, Appl. Phys. Lett. **69**, 1211 (1996).

[5] H. S. Chao, P. B. Griffin, J. D. Plummer, and C. S. Rafferty, Appl. Phys. Lett. **69**, 2113 (1996).

[6] P. A. Stolk, H.-J. Gossmann, D. J. Eaglesham, D. C. Jacobson, C. S. Rafferty, G. H. Gilmer, M. Jaraiz, J. M. Poate, H. S. Luftman, and T. E. Haynes, J. Appl. Phys. **81**, 6031 (1997).

[7] Y. H. Lee, Appl. Phys. Lett. **73**, 1119 (1998).

[8] N. Arai, S. Takeda, and M. Kohyama, Phys. Rev. Lett. **78**, 4265 (1997).

[9] N. Cuendet, T. Halicioglu, and W. A. Tiller, Appl. Phys. Lett. **68**, 19 (1996).

[10] J. L. Benton, K. Halliburton, S. Libertino, D. J. Eaglesham, and S. Coffa, J. Appl. Phys. **84**, 4749 (1998).

[11] N. E. B. Cowern, G. F. A. van de Walle, D. J. Gravesteijn, and C. J. Vriezema, Phys. Rev. Lett. **67**, 212 (1991).

[12] N. E. B. Cowern, K. T. F. Janssen, G. F. A. van de Walle, and D. J. Gravesteijn, Phys. Rev. Lett. **65**, 2434 (1990).

[13] R. B. Fair, in *Impurity Doping Processes in Si,* edited by F. F. Y. Wang (North-Holland, Amsterdam, 1981), p. 315.

[14] D. R. Lim, C. S. Rafferty, and F. P. Clemens, Appl. Phys. Lett. **67**, 2303 (1995).

[15] M. Jaraíz, L. Pelaz, E. Rubio, J. Barbolla, G. H. Gilmer, D. J. Eaglesham, H. J. Gossmann, and J. M. Poate, Mater. Res. Soc. Symp. Proc. **532**, 43 (1998).

[16] H. Bracht, E. E. Haller, and R. Clark-Phelps, Phys. Rev. Lett. **81**, 393 (1998).